Title

Superconductivity in Mo5SiB2

Permalink

https://escholarship.org/uc/item/8pk4g90t

Journal

Solid State Communications, 151(20)

ISSN

0038-1098

Authors

Machado, AJS
Costa, AMS
Nunes, CA
et al.

Publication Date

2011-10-01

DOI

10.1016/j.ssc.2011.07.005

Peer reviewed

Superconductivity in Mo$_5$SiB$_2$

A.J.S. Machado [a,b,*], A.M.S. Costa [a], C.A. Nunes [a], C.A.M. dos Santos [a], T. Grant [b], Z. Fisk [b]

[a] Escola de Engenharia de Lorena, Universidade de São Paulo, P.O. Box 116, Lorena, SP, Brazil
[b] Department of Physics and Astronomy, University of California at Irvine, Irvine, CA 92697, USA

ARTICLE INFO

ABSTRACT

In the Mo–Si binary system, Mo$_5$Si$_3$ crystallizes in the W$_5$Si$_3$ (T$_1$ phase) structure type. However, when boron replaces silicon in this compound, a structural transition occurs from the W$_5$Si$_3$ prototype structure to the Cr$_5$B$_3$ prototype structure (T$_2$ phase) at the composition Mo$_5$SiB$_2$. Mo$_5$SiB$_2$ has received much attention in the literature as a candidate for structural application in high-temperature turbines, but its electronic and magnetic behavior has not been explored. In this work, we show that Mo$_5$SiB$_2$ is a bulk superconducting material with critical temperature close to 5.8 K. The specific-heat, resistivity and magnetization measurements reveal that this material is a conventional type II BCS superconductor.

© 2011 Elsevier Ltd. All rights reserved.

1. Introduction

In the Nb–Si system, there are two phases with Nb$_5$Si$_3$ stoichiometry, the low-temperature αNb$_5$Si$_3$ phase (stable up to 1940 °C), isostructural with Cr$_5$B$_3$ (prototype), also named T_2 phase [1–3] and the high-temperature βNb$_5$Si$_3$ phase (stable from 1650 to 2520 °C), isostructural with W$_5$Si$_3$, named T_1 [1,2,4–6]. In the Mo–Si system, there exists only one phase at the Mo$_5$Si$_3$ stoichiometry, which is isostructural with W$_5$Si$_3$ (T_1). It is also common to find such structures in ternary RM–Si–B systems (RM—refractory metal: Nb, Mo, Ta, W) where there is a partial substitution of Si by B as represented by RM$_5$(Si, B)$_3$. The T_2 borosilicide variant of RM$_5$Si$_{(3-x)}$B$_{(x)}$ ($x = 0$–2) has been included in microstructural designs that yield useful structural materials due to a high-thermal stability associated with mixed metallic and covalent bonding within their complex crystal structure [7]. In addition to the atomic size factor, the effect of chemical bonding within the structure as expressed by parameters such as valence electron concentration per atom (e/a) has been shown to be essential in determining the stability of these phases [8–11]. The e/a criteria can also be correlated with the electronic structure of compounds which favor a high-cohesive energy [11]. The e/a ratio of the T_2 phase, varies in the range between 5.0 (corresponding to the Group VB metals such as Nb) and 6.0 (corresponding to the Group VIB metals such as Mo). In the Nb–Si–B ternary system, the T_2 phase can exist within the solubility range represented by

Nb$_5$Si$_{3-x}$B$_x$ with $0 \leq x \leq 2$ [12]. On the other hand, in the Mo–Si–B ternary system, the same T_2 phase exists only in the vicinity of the stoichiometry Mo$_5$SiB$_2$. This difference between the two systems is attributed to the extreme value of e/a ratio for the Mo borosilicide [11]. The Mo$_5$SiB$_2$ (T_2) has a body-centered tetragonal unit cell (space group I4/mcm), the unit cell containing 32 atoms (20 Mo, 4 Si, 8 B atoms) which are situated in a layered arrangement along the c axis. Three types of layers have been identified: layer A with only Mo atoms, layer B with only Si atoms, and layer C with a mixture of Mo and B atoms [13,14], forming a sequence MoB–Mo–Si–Mo–MoB, which is repeated in the lattice. The lattice parameters of this phase are $a = 5.99$ Å and $c = 11.02$ Å [14]. Superconductivity has been recently found in B-doped T_2 phase in the Nb–Si–B system [15], being the first evidence of superconductivity in a compound with the Cr$_5$B$_3$ prototype structure. Considering the existence of such a structure in a similar system (Mo–Si–B), it has been the aim of this work to examine the possible superconducting properties of the Mo$_5$SiB$_2$ (T_2) phase. Previous studies of the Mo–Si–B ternary system have primarily been interested in the development of alloys for high-temperature structural applications [11,16,17], and to our knowledge, have not studied the possibility of superconductivity in this system. The close similarity of Mo$_5$SiB$_2$ and Nb$_5$SiB$_2$ is shown here to include unambiguously bulk superconductivity with $T_c = 5.8$ K in Mo$_5$SiB$_2$.

2. Experimental procedure

Mo$_5$SiB$_2$ samples were prepared from a stoichiometric mixture of high purity Mo, Si and B via arc melting on a water-cooled Cu hearth under gettered high purity argon atmosphere. Each sample

---

* Corresponding author at: Escola de Engenharia de Lorena, Universidade de São Paulo, P.O. Box 116, Lorena, SP, Brazil. Tel.: +55 1231599911; fax: +55 1231533006.
E-mail address: jefferson@demar.eel.usp.br (A.J.S. Machado).

was remelted five times to ensure good chemical homogeneity. Due to sufficiently low vapor pressure of these constituent elements at melting temperature, the weight losses during arc melting were negligible (<0.5%). Some samples were prepared off-stoichiometry to check for possible homogeneity range of the T_2 phase. All as-cast samples were annealed at 1800 °C for 24 h under high vacuum, in order to reach thermodynamic equilibrium conditions. A diffractometer equipped with copper target for Cu Kα ($\lambda = 1.54056$ Å) radiation was used to acquire the powder X-ray diffraction patterns. The lattice parameters of the Mo_5SiB_2 phase were determined by using the PowderCell software [18]. Magnetic data were obtained using a commercial VSM-SQUID from Quantum Design. The temperature dependence of magnetization was obtained using a zero field cooling (ZFC) and Field Cooling (FC) conditions, under an applied magnetic field of 100 Oe. After both ZFC and FC measurements, M versus H data was acquired at 1.8 K. Electrical resistivity measurements were performed between 1.8 and 300 K using a conventional four probe system. The samples were irregular in shape and gold wires were spot-welded to the samples and served as the voltage and current leads. These measurements were carried out with and without applied magnetic field in order to estimate the upper critical field, using a PPMS apparatus (Quantum Design). The heat capacity (relaxation method) of a piece cut from one sample was determined in the 1.8–10 K range using a calorimetric probe inserted in the PPMS apparatus.

3. Results and discussion

The samples which were prepared off-stoichiometry had a two-phase microstructure, consistent with a small homogeneity range of the Mo_5SiB_2 phase [11]. However, the sample prepared at the exact Mo_5SiB_2 stoichiometry was single phase after the annealing procedure, as shown in Fig. 1 from the comparison of experimental and simulated diffractograms. The refined lattice parameters of the Mo_5SiB_2 were $a = 6.001$ Å and $c = 11.022$ Å, which is in good agreement with results reported in literature [14]. Magnetization as a function of temperature under ZFC and FC conditions is shown in Fig. 2. The ZFC curve demonstrates complete diamagnetic shielding; with a sharp superconducting transition close to 5.8 K (onset) and an estimated superconductor volume near 120%. The deviation from the expected value $-1/4\pi$ (100%) is due to the irregular shape of the sample which makes difficult determining the correct demagnetization factor. The difference in results between ZFC and FC conditions indicates a type II superconductor and points to a weak Meissner effect due to strong flux pinning. The $M(T)$ is independent of T in the normal state which is indicative of a Pauli-paramagnetism. The type II behavior is clear in the inset of Fig. 2 which shows M vs H data at 1.8 K, and from which could be determined the lower and upper critical field values, H_{c1} and H_{c2} respectively. The lower critical field (H_{c1}) was estimated through the deviation from linearity in the M vs H curve while the upper critical field (H_{c2}) value could be defined at the point where the magnetization signal enter the normal state. Thus, the values of H_{c1} and H_{c2} are 232 Oe and 5.5 kOe respectively at 1.8 K. In order to obtain the dependence of both critical fields with temperature, M vs H measurements were carried out at several temperatures and the data plotted in Fig. 3. Using the procedure above, H_{c1} and H_{c2} values could be determined as a function of temperature. The inset shows estimated H_{c1} values by the horizontal arrows, determined from the points where the curves deviate from linearity. The definition of the H_{c2} is represented by the vertical arrow in Fig. 3 used to exemplify how H_{c2} was estimated in each temperature. Fig. 4 shows H_{c2} vs T and H_{c1} vs T, determined from M vs H (Fig. 3 open circle and triangle). The upper critical field at 0 K ($\mu_o H_{c2(0)}$), estimated using the WHH
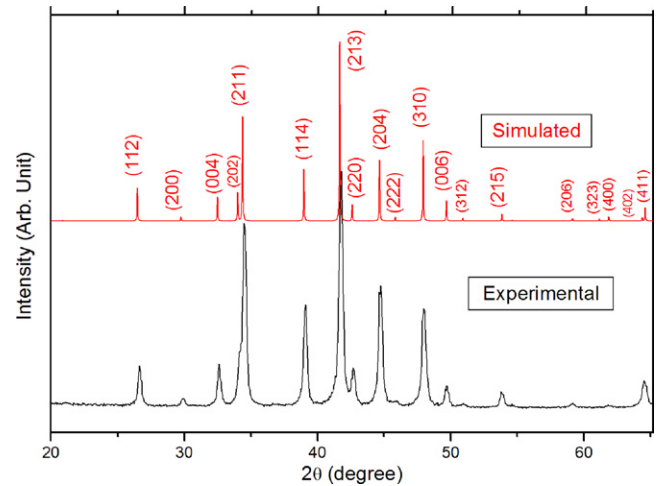

Fig. 1. Comparison between the diffraction patterns: experimental (black line) and simulated (red line) show good agreement. (For interpretation of the references to colour in this figure legend, the reader is referred to the web version of this article.)
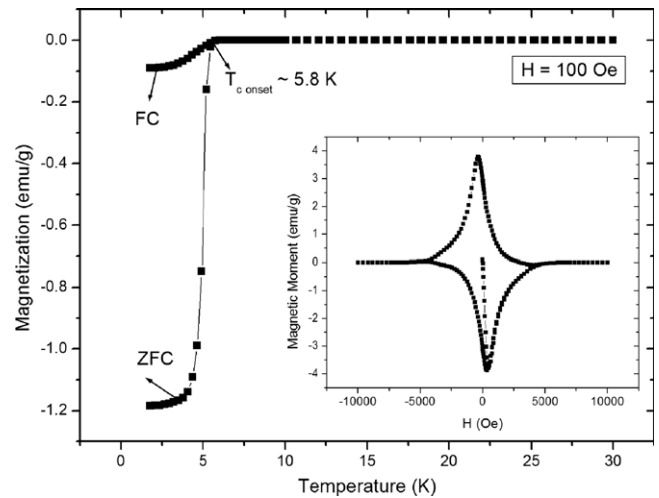

Fig. 2. Magnetization as a function of temperature under ZFC and FC conditions at 100 Oe, displaying a clear superconducting transition close to 5.8 K. Inset displays the M vs H curve at 1.8 K, where we observe a type II superconductor behavior.

formula [19] in the limit of short electronic mean-free path (dirty limit) is given by:

$$\mu_o H_{c2}(0) = -0.693 T_c (dH_{c2}/dT)_{T=Tc}.$$

Fig. 4 shows the solid line expected in the WHH model, which fits the data very well and leads to a $\mu_o H_{c2}(0)$ value of 0.606 T or $H_{c2}(0) \sim 6060$ Oe. Hence, pair breaking in Mo_5SiB_2 is probably caused by orbital fields [19]. The fitting from Fig. 4 data allows an estimation of the coherence length through the Ginzburg–Landau (GL) formula, $\mu_o H_{c2}(0) = \frac{\phi_o}{2\pi \xi_0^2}$, where ϕ_o is a quantum flux equal to 2.068×10^{-15} T. m^{-2}, yielding $\xi_o \sim 233$ Å. From Fig. 4 it is possible to estimate the penetration depth through the formula $H_{c1} = \frac{\phi_o}{2\pi \lambda_L^2}$, where the λ_L parameter represents the penetration depth. Analysis of the data in Fig. 4 suggests a lower critical field at 0 K of $H_{c1} \sim 262$ Oe which yields $\lambda_L \sim 112$ nm. These results yield a GL factor of approximately $\kappa_{(0)} \sim 4.8$, which is higher than $\frac{1}{\sqrt{2}}$ and suggests type II superconductivity. The electrical resistance of Mo_5SiB_2 as a function of temperature is shown in Fig. 5 and exhibits a sharp superconducting transition close to 5.8 K (onset), consistent with the results presented in
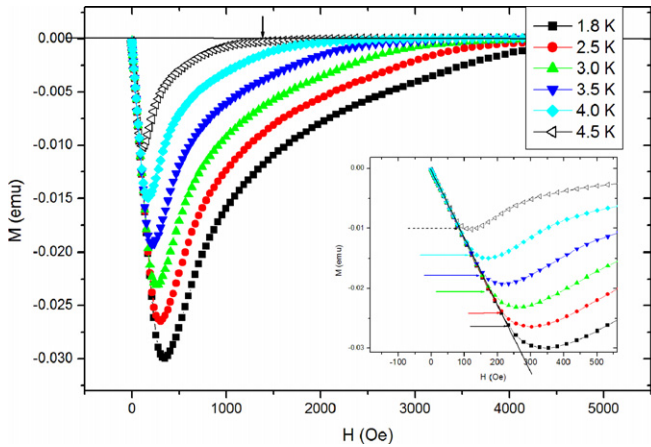
Fig. 3. M versus H for several isotherms 1.8, 2.5, 3.0, 3.5, 4.0 and 4.5 K. The inset shows the definition of the lower critical field (H_{c1}), which can be estimated through the deviation from linearity, represented by a horizontal arrow. The definition of the upper critical field is represented by a vertical arrow.
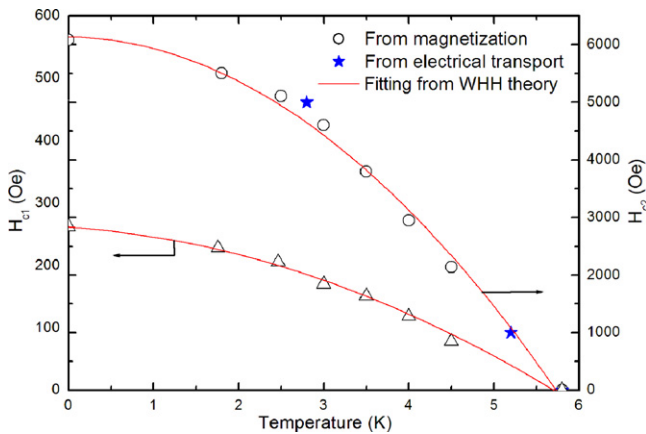

Fig. 4. H_{c1} and H_{c2} versus temperature. The H_{c2} was extracted from magnetization and resistivity measurements which show good agreement with WHH model (red line). (For interpretation of the references to colour in this figure legend, the reader is referred to the web version of this article.)

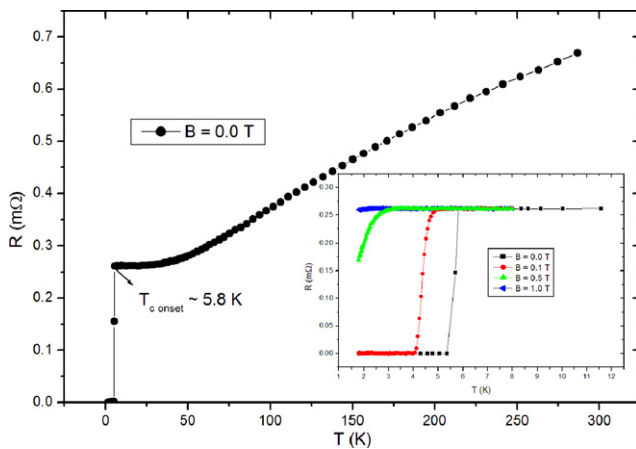**Fig. 5.** R vs T in zero magnetic field shows the superconducting critical temperature close to 5.8 K (onset), which is the same temperature observed in Fig. 2. The inset shows a magnetoresistance for various applied magnetic field in $0 \leq \mu_o H \leq 1.0$ T interval.

Fig. 2. The inset of Fig. 5 displays the magnetoresistance behavior and shows the dependence of the critical temperature in applied magnetic field. The shift in superconducting critical temperature

is consistent with the estimated value from Fig. 3. Indeed, the H_{c2} as a function of temperature estimated from electrical transport measurements follows very closely the fitting curve of the WHH model as shown in Fig. 4. The results obtained from these different techniques are in good agreement and reveal the good quality and stability of the sample. The heat capacity data is shown in Fig. 6 where C/T is plotted against T^2 at zero magnetic field. The normal state can be fit to the expression $C_n = \gamma T + \beta T^3$ by a least-square analysis, which yields the value $\gamma = 16.98$ (mJ/mol K^2) and $\beta = 0.114$ (mJ/mol K^4). This β value corresponding to Debye temperature $\Theta_D \sim 515$ K and the relatively high value of Sommerfeld coefficient suggests a modest density of states per atom at the Fermi level. Our result shows that Mo_5SiB_2 is unambiguously a bulk superconductor. The subtraction of the phonon contribution allows us to evaluate the electronic contribution to the specific-heat, plotted as C_e/T vs T in Fig. 7. An analysis of the jump yields $\Delta C_e/\gamma_n T_c \sim 1.39$ which is very close to weak coupling BCS prediction (1.43). The energy gap is obtained from a plot of $\ln(C_s)$ vs $1/T$ as shown in the inset of Fig. 7. The linear behavior obeys the expression $\ln(C_s) = 6.87$–$7.972/T$. Through this linear fitting we estimate an energy gap of 0.69 meV which represents the BCS weak coupling limit. The gamma value extracted from Fig. 6 is proportional to the density of states (DOS) at Fermi level through $\gamma = \frac{\pi^2}{3} k_B^2 N(\varepsilon_F)$, where $N(\varepsilon_F)$ represents the DOS at Fermi level. As Sommerfeld coefficient is proportional to the $N(\varepsilon_F)$, we would expect a peak in the density of states at Fermi level of the band structure of this material. Indeed, the band structure calculation showed a peak in the density of states close to Fermi level in accordance with reference [11]. Assuming that this compound is a conventional BCS superconductor, as evidenced by the results shown in this work, the superconducting critical temperature must increase with $N(\varepsilon_F)$. As discussed in the introduction, $Nb_5Si_{3-x}B_x$ has a large solubility limit with boron content varying from $x = 0$ to $x = 2$ [15]. Thus the Nb_5SiB_2 compound presents the opportunity to compare the Sommerfeld coefficient with the superconducting critical temperature in both. Heat capacity data for Nb_5SiB_2 is shown in Fig. 8 where one can observe a gamma value of 3.5 (mJ/mol K^2). This value is about 21% of the observed value for Mo_5SiB_2 in this paper. However, Nb_5SiB_2 has a superconducting critical temperature close to 7.2 K. Although both compounds have the same crystalline structure, their electron counts differ and the lower density of states in Nb_5SiB_2 is perhaps not unexpected, but the higher critical temperature given the much lower density of states is somewhat surprising. $N(\varepsilon_F)$ can increase significantly in a material with saddle points in the energy dispersion on the electronic structure, the so called Van Hove singularities [20]. This apparent "discrepancy" in T_c between the two compounds may be related with the layered characteristic (quasi-2D) of this family of compounds. If a rigid-band model is applicable, the Fermi level can be shifted through the appropriate choice of RM (Refractory Metal) to a maximum of $N(\varepsilon_F)$ [21–24]. Then perhaps this apparent "discrepancy" between T_c and density of states might be described by the Van Hove scenario [20]. In fact, this Van Hove scenario, where the maximum in the DOS is ideally localized at ε_F, was used to explain the high superconducting critical temperature in intermetallics $A15$ superconductor materials [25]. All results from specific-heat suggesting that Mo_5SiB_2 is a conventional BCS superconductor material. In all BCS superconductors the Cooper-pairing is a phonon mediated and we can determine the dimensionless electron–phonon coupling constant λ with the McMillan relation [26].

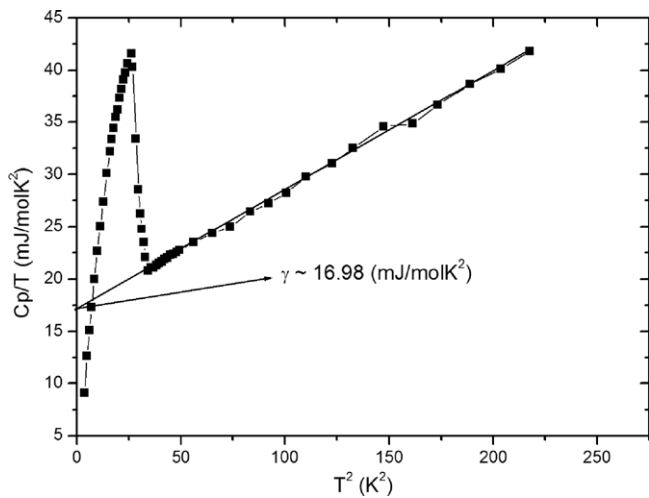$$T_c = \frac{\theta_D}{1.45} \exp\left[\frac{-1.04(1+\lambda)}{\lambda - \mu_c^*(1+0.62\lambda)}\right].$$

Fig. 6. C/T vs T^2 curve at zero magnetic field shows the superconducting critical temperature close to 5.8 K, which is consistent with the electrical transport and magnetization measurements. The solid line is the fit of the experimental data to $c = \gamma T + \beta T^3$ between 1.8 and 15.0 K.
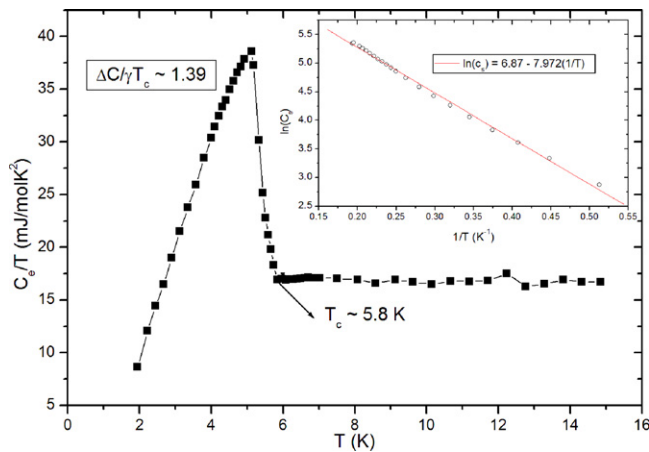

Fig. 8. Cp/T vs T^2 curve at zero magnetic fields for Nb$_5$SiB$_2$, which shows superconducting critical temperature close to 7.2 K. The solid line is the fit of experimental data to $c = \gamma T + \beta T^3$ between 1.8 and 10.0 K.

material in the BCS weak coupling limit. Finally these results suggest that Cr$_5$B$_3$ prototype structure is a promising structure for superconductivity and other compounds with the same prototype structure should be investigated.

Fig. 7. Temperature dependence of the electronic specific-heat divided by temperature (C_e/T). The inset shows the fitting of the ln(C_s) against temperature reciprocal.

Taking the Coulomb coupling constant μ_c^* to be 0.13, a usual value, and $\theta_D = 515$ K estimated through β value from specific-heat measurement, we get $\lambda = 0.572$, which is in good agreement with values from others conventional superconductor materials [27].

4. Conclusions

In summary, the structural, magnetic, electronic transport and specific-heat properties have been investigated in Mo$_5$SiB$_2$. The excellent agreement of transition temperature as characterized by the magnetic, resistivity and specific-heat data unambiguously indicates that the polycrystalline Mo$_5$SiB$_2$ compound is a bulk superconductor material with critical temperature $T_c \sim 5.8$ K. The comparison between superconducting properties of the Nb$_5$SiB$_2$ and Mo$_5$SiB$_2$ compounds shows that the critical temperature does not increase with the increasing of DOS at Fermi level. This apparent divergence may be related to a possible Van Hove singularity. The Mo$_5$SiB$_2$ is a conventional superconductor
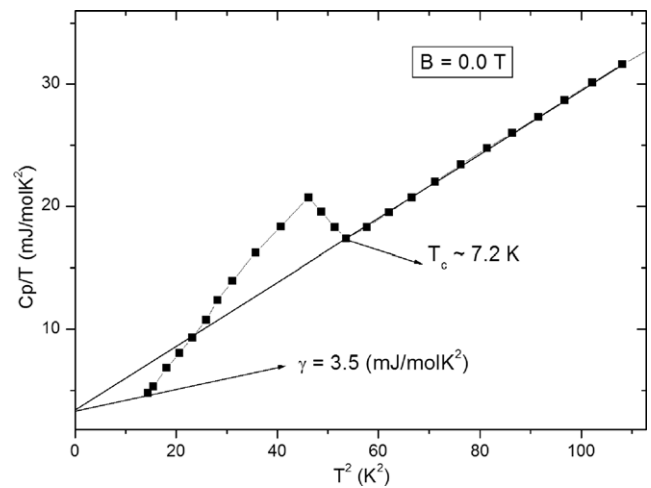
References

[1] T.B. Massalski (Ed.), Binary Alloy Phase Diagrams, 2nd ed., Materials Park, OH, 6, 1990, 7.
[2] A.G. Knapton, Nature 175 (1955) 730.
[3] E. Parthé, B. Lux, H. Nowotny, Monatsh. Chem. 86 (1955) 859.
[4] E. Parthé, H. Nowotny, H. Schmid, Monatsh. Chem. 86 (1955) 385.
[5] E. Parthé, H. Schachner, H. Nowotny, Monatsh. Chem. 86 (1955) 182.
[6] A.N. Christensen, Acta Chem. Scand. A 37 (1983) 519–522.
[7] A.K. McMahan, J.E. Klepeis, M. Schifgaarde, M. Methfessel, Phys. Rev. B 50 (1994) 10742.
[8] C.L. Fu, A.J. Freeman, T. Oguchi, Phys. Rev. Lett. 54 (1985) 2700.
[9] S. Ohnishi, A.J. Freeman, M. Weinert, Phys. Rev. B 28 (1983) 6741.
[10] J. Xu, A.J. Freeman, Phys. Rev. B 40 (1989) 11927.
[11] R. Sakidja, J.H. Perepezko, S. Kim, N. Sekido, Acta Materialia 56 (2008) 5223.
[12] G. Rodrigues, C.A. Nunes, P.A. Suzuki, G. Coelho, Intermetallics 12 (2004) 181.
[13] H. Nowotny, E. Dimakopoulou, H. Kudielka, Monatsh. Chem. 88 (1957) 180.
[14] B. Aronsson, Acta Chem. Scand. 12 (1958) 31.
[15] A. Brauner, C.A. Nunes, A.D. Bortolozo, G. Rodrigues, A.J.S. Machado, Solid. Stat. Comm. 149 (2009) 467.
[16] D.M. Dimiduk, J.H. Perepezko, MRS Bull. 28 (2003) 639.
[17] J.H. Perepezko, C.A. Nunes, S.H. Yi, D.J. Thoma, High Temperature Oerdered Intermetallic Alloys VII, MRS, Pittsburg, PA, 1997.
[18] Kraus, G. Nolze, J. Appl. Cryst. 29 (1996) 301.
[19] N.R. Werthamer, E. Helfand, P.C. Hohenberg, Phys. Rev. 147 (1966) 295.
[20] L. van Hove, Phys. Rev. B 89 (1953) 1189.
[21] M.A.S. Boff, G.L.F. Fraga, D.E. Brandão, A.A. Gomes, T.A. Grandi, Phys. Status A 154 (1996) 549.
[22] W. Lin, A.J. Freeman, Phys. Rev. B 45 (1992) 61.
[23] M.A.S. Boff, G.L.F. Fraga, D.E. Brandão, A.A. Gomes, J. Magn. Magn. Matter. 153 (1996) 135.
[24] Jurgen Winterlik, Gerhard H. Fecher, Claudia Felser, Martin Jourdan, Kai Grube, Frédéric Hardy, Hilbert von Lohneysen, K.L. Holman, R.J. Cava, Phys. Rev. B 78 (2008) 184506.
[25] J. Labbé, J. Friedel, J. Phys. France 27 (1966) 153.
[26] W.L. McMillan, Phys. Rev. B 167 (1968) 331.
[27] P. Roedhammer, E. Gmelin, W. Weber, J.P. Remeika, Phys. Rev. B 15 (1977) 711.